HHS Public Access

Author manuscript

Small. Author manuscript; available in PMC 2017 May 01.

Published in final edited form as:

Small. 2016 May ; 12(20): 2775–2782. doi:10.1002/smll.201600194.

Dynamic Positron Emission Tomography Imaging of Renal Clearable Gold Nanoparticles

Dr. Feng Chen,
Department of Radiology, University of Wisconsin – Madison, WI, USA

Shreya Goel,
Materials Science Program, University of Wisconsin - Madison, WI, USA

Reinier Hernandez,
Department of Medical Physics, University of Wisconsin - Madison, WI, USA

Stephen A. Graves,
Department of Medical Physics, University of Wisconsin - Madison, WI, USA

Sixiang Shi,
Materials Science Program, University of Wisconsin - Madison, WI, USA

Robert J. Nickles, and
Department of Medical Physics, University of Wisconsin - Madison, WI, USA

Prof. Weibo Cai*
Department of Radiology, University of Wisconsin – Madison, WI, USA, Department of Medical Physics, University of Wisconsin - Madison, WI, USA, University of Wisconsin Carbone Cancer Center, Madison, WI, USA

Abstract

Optical imaging has been the primary imaging modality for nearly all of the renal clearable nanoparticles since 2007. Due to the tissue depth penetration limitation, providing accurate organ kinetics non-invasively has long been a huge challenge. Although a more quantitative imaging technique has been developed by labeling nanoparticles with single-photon emission computed tomography (SPECT) isotopes, the low temporal resolution of SPECT still limits its potential for visualizing the rapid dynamic process of renal clearable nanoparticles *in vivo*. Here, we report the dynamic positron emission tomography (PET) imaging of renal clearable gold (Au) nanoparticles by labeling them with copper-64 (^{64}Cu) to form ^{64}Cu-NOTA-Au-GSH. Systematic nanoparticle synthesis and characterizations were performed to demonstrate the efficient renal clearance of as-prepared nanoparticles. A rapid renal clearance of ^{64}Cu-NOTA-Au-GSH was observed (>75 %ID at 24 h post-injection) with its elimination half-life calculated to be less than 6 min, over 130 times shorter than previously reported similar nanoparticles. Dynamic PET imaging not only addresses the current challenges in accurately and non-invasively acquiring the organ kinetics, but also

Fax: (+1) 608-265-0614, ; Email: WCai@uwhealth.org, Homepage: http://mi.wisc.edu.
F. Chen, S. Goel and R. Hernandez contributed equally to this work

Supporting Information
Supporting Information is available from the Wiley Online Library or from the author.

potentially provides a highly useful tool for studying renal clearance mechanism of other ultra-small nanoparticles, as well as the diagnosis of kidney diseases in the near future.

Keywords

Dynamic imaging; Positron emission tomography; Gold nanoparticle; Renal clearance

1. Introduction

Although promising pre-clinical cancer diagnostic and therapeutic results have been reported repeatedly using various kinds of sophisticated nanomaterials,[1–7] most of them might still hold little potential for future clinical translation due to limitations such as high (>30 %ID/g) and long-term (>months) accumulation of nanoparticles in the reticuloendothelial system, difficulties in establishing large-scale good manufacturing practice (GMP), lack of highly specific disease (such as tumor) targeting capability, *etc.* Encouraged by the successful approval of C dots (which are ultra-small dye-encapsulated and RGD-conjugated fluorescence silica nanoparticles) as Investigational New Drug (IND) by the Food and Drug Administration (FDA) and their ongoing human clinical trials,[8–10] engineering of multifunctional, renal clearable and tumor targeted inorganic nanoparticles has emerged as a promising research direction in the field of nano-oncology.[11]

Compared with C dots, ultra-small (2–3 nm sized) glutathione (GSH) coated luminescent gold (Au) nanoparticle (*i.e.* Au-GSH) is a relatively new type of renal clearable inorganic nanoparticle designed for future cancer targeted multimodality imaging.[12–15] Although *in vivo* active targeting of Au-GSH has not been achieved yet, by modifying the nanoparticles with poly(ethylene glycol) (molecular weight: 1 kDa), researchers have successfully demonstrated the existence of enhanced permeability and retention (EPR) effect after injecting Au-PEG_{1k} in tumor-bearing mice.[12] Since the pioneering work of renal clearable quantum dots (QDs) in 2007,[16] optical imaging has been the primary imaging modality for nearly all of the renal clearable nanoparticles including Au-GSH (Table S1). To address the semi-quantitative limitation of optical imaging (which might result in lack of accuracy when studying the pharmacokinetics of nanoparticles *in vivo*), Au-GSH nanoparticles that have been intrinsically radiolabeled with a single-photon emission computed tomography (SPECT) isotope, *i.e.* gold-198 (^{198}Au, $t_{1/2}$=2.7 d), have also been developed.[14] Despite the fact that SPECT is capable of a deep tissue imaging and quantification, the low temporal resolution limits its potential for visualizing the dynamic process of Au-GSH *in vivo*. Although optical imaging might, to a certain degree, play a complementary role, so far, great challenges still exist in providing the dynamic information of Au-GSH in the early stage (within the first 30 min post-injection), and the accurate kinetics of nanoparticles in different organs (especially heart, liver and kidney).

Here, we report the dynamic positron emission tomography (PET) imaging of renal clearable Au nanoparticles by labeling them with copper-64 (^{64}Cu, a positron emission radioisotope with a 12.7 h half-life) to form ^{64}Cu-NOTA-Au-GSH (where NOTA is the chelator used for ^{64}Cu labeling). Dynamic PET imaging of ^{64}Cu-NOTA-Au-GSH involved

the collection of a series of frames of data over contiguous time intervals ranging from the first 5 s to 60 min post-injection. Data from each of the frames was independently reconstructed to form a set of images. These images were then used to create the dynamic process (a short video showing the rapid distribution and elimination of nanoparticles), plot the organ kinetics, as well as estimate the physiological parameters, such as the distribution and elimination half-life of ^{64}Cu-NOTA-Au-GSH.

2. Results and Discussions

2.1. Synthesis of Ultra-small Radio-labeled Au Nanoparticles

The synthesis of ultra-small Au-GSH was achieved by using procedures reported previously with a simplified purification process.[14–15] In a typical synthesis, reduced glutathione (~0.24 mmol) was first mixed with gold(III) chloride trihydrate ($HAuCl_4 \cdot 3H_2O$, ~0.24 mmol) in water at room temperature, followed by adding 30 μL of 1 M $HAuCl_4 \cdot 3H_2O$. The mixture was then transferred to a 90 °C water bath and kept reacting for 35 min. Before purifying the nanoparticles, a 10 kDa Amicon centrifugal filter was used to concentrate as-synthesized Au-GSH. The nanoparticles were then passed through a PD-10 column using phosphate buffered saline (PBS) as the mobile phase. Size and size distribution of Au-GSH in different eluted fractions were found to be different. Fractions 2.5–3.5 mL contained nanoparticles (Au concentration: ~0.9 mg/mL) with a nearly spherical morphology (Figure 1a) and a hydrodynamic (HD) size of 2.5 ± 0.1 nm (polydispersity index: 0.346, Figure 1b), while other fractions contained nanoparticles with a broad size distribution, as shown in Figure S1. As reported previously, ultra-small Au-GSH also exhibited near infrared emission with a maximum emission peak located at around 800–810 nm.[14] Figure S2 further provides the optical emission intensity curve of Au-GSH from different fractions (*Ex=430 nm, Em=800 nm*). Only light yellow colored 2–3 nm sized Au-GSH nanoparticles obtained from fractions 2.5–3.5 mL were used for the following studies.

As demonstrated by previous research,[15] the surface of as-synthesized Au nanoparticles was capped with a layer of glutathione (a tripeptide) which protect nanoparticle from aggregation (and degradation) in the blood stream. The presence of amine groups from the Au-GSH surface was confirmed by a ninhydrin test, which showed an obvious blue color after mixing Au-GSH with ninhydrin test kit reagents (Figure 1a, inset). The conjugation of NOTA to Au-GSH was then achieved by reacting p-SCN-Bn-NOTA with Au-GSH in dimethyl sulfoxide to form NOTA-Au-GSH. The dynamic light scattering (DLS) measurement showed only a slightly increased HD size from 2.5 ± 0.1 to 2.6 ± 0.1 nm (Figure 1b) after NOTA conjugation. The labeling yield of ^{64}Cu to NOTA-Au-GSH was estimated to be over 90% after incubating NOTA-Au-GSH with ^{64}Cu at 37 °C for 30 min. A good co-localization between radioactive intensity and luminescent intensity of ^{64}Cu-NOTA-Au-GSH (as shown in Figure 1c) clearly demonstrated the successful synthesis of ^{64}Cu-NOTA-Au-GSH.

2.2. Renal Clearance of Ultra-small Au Nanoparticles

Before *in vivo* dynamic PET imaging, systematic characterizations were performed to demonstrate the renal clearance of as-prepared ^{64}Cu-NOTA-Au-GSH. Serum stability was

first carried out to ensure its high radio-stability. Our results showed that 98% of ^{64}Cu was still found intact after incubating ^{64}Cu-NOTA-Au-GSH with whole mouse serum at 37 °C for 1 h, and only less than 5% of ^{64}Cu was detached after 24 h incubation (Figure S3), clearly indicating high radio-stability of ^{64}Cu-NOTA-Au-GSH *in vitro*. To demonstrate the renal clearance of ^{64}Cu-NOTA-Au-GSH *in vivo*, as-synthesized nanoparticles were intravenously injected into healthy BALB/c mice and imaged with PET 2 h post-injection. The PET/CT image in Figure 2a showed the expected dominant uptake of nanoparticles in the bladder (*marked with a yellow arrow*) and kidneys (*marked with red arrows*). No noticeable contrast enhancement in CT imaging was observed since mice were injected with a highly diluted dose of Au nanoparticles.

Since Au-GSH itself can be used as a CT enhancement contrast agent (as we also demonstrated in Figure S4), to further confirm the renal clearance of nanoparticles using CT imaging, a concentrated dose of NOTA-Au-GSH (cold, ~0.5 mg Au per mouse) was mixed with ^{64}Cu-NOTA-Au-GSH (hot) and injected into the mice. A clear accumulation of NOTA-Au-GSH and enhanced CT intensity in mouse bladder was observed in this case, as shown in Figure 2b (the CT image). In both cases, nanoparticles cleared really fast with significantly reduced radioactivity *in vivo* at 19 h post-injection, as shown in Figure 2c and d. By taking advantages of the intrinsic optical imaging property, we showed another evidence of renal clearance by performing *ex vivo* optical and PET imaging at 30 min post-injection (Figure S5). A good co-localization of optical and PET signals in kidneys (and other organs) not only indicate the clearance of nanoparticles *via* the renal pathway, but also the intactness of ^{64}Cu-NOTA-Au-GSH *in vivo*. To further demonstrate that non-radiolabeled NOTA-Au-GSH nanoparticles also remained intact with their intrinsic fluorescent properties after excretion into urine, we further provided the optical imaging of NOTA-Au-GSH in mouse urine samples using IVIS Spectrum (*Ex=430 nm, Em=800 nm*) at different post-injection time points (from 4 h to 48 h, as shown in Figure S6).

A metabolic cage study was then performed to quantitatively study the renal and hepatic clearance rates of ^{64}Cu-NOTA-Au-GSH in mice (n=3). Mice were injected with ^{64}Cu-NOTA-Au-GSH and kept in metabolic cages. Urine and feces were collected separately at different time points (*e.g.* 6, 16 and 24 h post-injection) with their radioactivities counted using a gamma counter. Although we believe over 50 %ID of injected ^{64}Cu-NOTA-Au-GSH was cleared through the bladder within the first 2 h (based on the *in vivo* PET imaging studies), due to the difficulties in collecting mouse urine during the early time points, the earliest time point we could provide is 6 h post-injection. Inset in Figure 3a and Table S2 show quantitatively the amount of nanoparticles cleared in mouse urine and feces. Dominant renal clearance was again observed with the urine uptake measured to be 64.9 ± 10.2 %ID (at 6 h post-injection), which was nearly 50 times higher than that of in mouse feces (1.3 ± 0.1 %ID). A slight increase in urine uptake was also observed with the number found to be 72.6 ± 10.3 %ID at 24 h post-injection. The total clearance (including renal and hepatic clearance) of ^{64}Cu-NOTA-Au-GSH was estimated to be over 75 %ID at 24 h post-injection. To estimate the uptake of nanoparticles in different organs, the mice were sacrificed with all major organs collected, wet-weighted, and counted with a gamma counter after 24 h. Figure 3a and Table S3 present the *ex vivo* biodistribution of ^{64}Cu-NOTA-Au-GSH in mice. Numbers were presented as percentage of the injected dose (%ID). Besides the dominant

accumulation of nanoparticles in urine and feces, nanoparticle uptake in liver and kidney were found to be 0.99 ± 1.11 %ID and 0.86 ± 0.42 %ID, respectively. A separate biodistribution study was also performed to provide a more detailed distribution information of ^{64}Cu-NOTA-Au-GSH in mice. Numbers were presented as percentage of the injected dose per gram (%ID/g) in this case. As shown in Figure 3b and Table S4, the majority of ^{64}Cu-NOTA-Au-GSH was found in mouse kidney and liver with their uptake measured to be 1.69 ± 0.54 and 0.33 ± 0.22 %ID/g, respectively, which were 4 and ~9 times lower than that of previously reported [^{198}Au]Au-GSH (kidney: 6.83 ± 0.98 %ID/g; liver: 2.95 ± 0.51 %ID/g) with a comparable particle size distribution (HD: 2–3 nm).[14]

2.3. Dynamic PET imaging of Radio-labeled Au Nanoparticles

To study the dynamic PET imaging, a group of mice (n=4) were injected with 5–10 MBq of ^{64}Cu-NOTA-Au-GSH and imaged in a microPET/microCT Inveon rodent model scanner. A 60-min dynamic scan was performed and framed into 46 frames: 12×5 s, 6×10 s, 6×30 s, 10×60 s, 6×150 s, 5×300 s. Figure 4 shows the selected frames of maximum intensity projection (MIP) images from the dynamic PET imaging. *Video S1* shows the rapid clearance of ^{64}Cu-NOTA-Au-GSH during the first 60 min after injecting to healthy BALB/c mice.

Our results showed an instant uptake (39.1 ± 26.4 %ID/g) of ^{64}Cu-NOTA-Au-GSH in the heart at 8 s post-injection. The heart uptake was almost doubled (66.3 ± 6.7 %ID/g) within the next 4 s before it started to decrease over time (Figure 4, *FRAME-3*). Uptake of nanoparticles in the liver continued to increase for the first 27 s (Figure 4, *FRAME-7*), and peaked at 23.2 ± 1.1 %ID/g, while it took about 105 s for uptake in kidneys to reach their maximal values (57.3 ± 5.6 %ID/g for left kidney and 52.9 ± 11.7 %ID/g for right kidney, Table S6, *FRAME-17*). Kidney and bladder became the dominant uptake organs after 2 min post-injection with the nanoparticles clearing rapidly *via* the renal system, as shown from *FRAME-19* to *FRAME-46* (Figure 4, Table S6–S9). As expected, the bladder uptake continued to increase throughout the whole dynamic imaging process, with the highest uptake estimated to be 252.6 ± 114.5 %ID/g (at 57.5 min post-injection). Less than 3 %ID/g of liver uptake and less than 6 %ID/g of kidney were observed at the end of dynamic PET imaging (Figure 4, *FRAME-46*).

A static PET imaging of the same mice at 12 h and 24 h post-injection was also performed to provide a more complete clearance picture of ^{64}Cu-NOTA-Au-GSH (Video S2). Our ROI analysis showed a significantly reduced liver and kidney uptake down to 0.94 ± 0.12 and 1.60 ± 0.14 %ID/g at 24 h post-injection, respectively, which matched very well with that obtained from our *ex vivo* biodistribution study (liver: 0.33 ± 0.22 %ID/g, kidney: 1.69 ± 0.54 %ID/g, Figure 3b and Table S4).

2.4. Organ Kinetics of Radio-labeled Au Nanoparticles

Due to the depth penetration limitation of optical imaging, providing accurate organ kinetics non-invasively has long been a huge challenge for most of the non-radiolabeled renal clearable nanoparticles. Although heart kinetics has been calculated by sampling the blood and quantifying the nanoparticles concentrations (by running inductively coupled plasma

mass spectroscopy) at selected time points,[12, 15] many mice need to be sacrificed if one needs to obtain an accurate kidney (or liver) kinetics. Quantitative analysis of the dynamic PET imaging data holds potential to provide more accurate kinetics of nanoparticles in major clearance organs without sacrificing the animals. Figures 5a to 5e show the detailed time-activity curves of ^{64}Cu-NOTA-Au-GSH in organs of heart, kidneys, liver and bladder. By comparing the kidney kinetics of ^{64}Cu-NOTA-Au-GSH in both healthy mice and mice with acute kidney injury (AKI, also known as acute renal failure, or ARF), dynamic PET imaging of ^{64}Cu-NOTA-Au-GSH could become a highly useful tool for a quick diagnosis of kidney diseases in the future.

The clearance rate of ^{64}Cu-NOTA-Au-GSH from the blood compartment was later determined by fitting the dynamic time-activity curves of the heart to a two-phase exponential decay (as shown in Figure 5f and Figure S7). The initial distribution half-life ($t_{1/2\alpha}$) of the ^{64}Cu-NOTA-Au-GSH was found to be 0.7 ± 0.1 min, which was >7 times shorter than previously estimated value (5.4 ± 1.2 min for Au-GSH).[12, 14] This was confirmed with the rapid distribution of ^{64}Cu-NOTA-Au-GSH in mice, as shown in Figure 4, Table S5 and Video S1. Surprisingly, the elimination half-life ($t_{1/2\beta}$) that was obtained by fitting the time activity curve was 5.8 ± 0.8 min, which was >130 times shorter than [^{198}Au]Au-GHS with a similar HD size (2–3 nm, $t_{1/2\beta}$=12.7 h or 762 min).[14] For the first time, we also showed the kinetics of renal clearable nanoparticles in mouse kidneys and liver. The elimination half-life of nanoparticles in kidney was estimated to be in the range of 8 to 11 min (Figure 5f, Figure S8), which was slightly longer than that of in liver (~7 min, Figure S9). Taken all together, we demonstrated the successful synthesis and dynamic PET imaging of renal clearable ^{64}Cu-NOTA-Au-GSH, which not only provide us a more detailed clearance picture of nanoparticles *in vivo*, but also more accurate clearance kinetics of nanoparticles in major organs.

3. Conclusion

In conclusion, we reported the dynamic PET imaging of radiolabeled renal clearable Au nanoparticles. A rapid renal clearance of ^{64}Cu-NOTA-Au-GSH was observed with its elimination half-life calculated to be >130 times shorter than previously reported similar nanoparticles. Dynamic PET imaging not only addresses the current challenges in accurately and non-invasively acquiring the organ kinetics, but also provides a highly useful tool for studying other renal clearance mechanism of ultra-small nanoparticles, as well as the diagnosis of kidney diseases in the future.

4. Experimental Section

Materials

Gold(III) chloride trihydrate (>99.9%), reduced glutathione (>98.0%) were purchased from Sigma-Aldrich (St. Louis, MO). p-SCN-Bn-NOTA (i.e., 2-S-(4-isothiocyanatobenzyl)-1,4,7-triazacyclononane-1,4,7- triacetic acid) was acquired from Macrocyclics, Inc. (Dallas, TX). PD-10 columns were purchased from GE Healthcare (Piscataway, NJ). 10 kDa Amicon centrifugal filters were purchased from Merck Millipore Ltd. Water and all buffers were of

Millipore grade and pretreated with Chelex 100 resin to ensure that the aqueous solution was free of heavy metals. All chemicals were used as received without further purification.

Characterizations

Transmission electron microscopy (TEM) images were obtained on a FEI T12 microscope operated at an accelerating voltage of 120 kV. Standard TEM samples were prepared by dropping diluted products onto carbon-coated copper grids. Dynamic light scattering was performed on Nano-Zetasizer (Malvern Instruments Ltd.). Biodistribution studies were performed by measuring the radioactivity in the tissue in a WIZARD^2 gamma-counter (Perkin-Elmer). Optical imaging was performed by using an IVIS Spectrum Preclinical *in vivo* imaging system (*Ex*=435 nm, *Em*=800 nm).

Synthesis of 2–3 nm sized Au-GSH

The synthesis of ultra-small Au-GSH was achieved by using procedures reported previously with a simplified purification process.[14–15] In a typical synthesis 2–3 nm sized Au-GSH, 73.8 mg (~0.24 mmol) of reduced glutathione (GSH) together with 94.5 mg (~0.24 mmol) of gold(III) chloride trihydrate ($HAuCl_4 \cdot 3H_2O$) in 10 mL of water at room temperature. Then, in 10 mL of GSH/Au mixture, add 30 μL of 1 M $HAuCl_4 \cdot 3H_2O$. The mixture was then transferred to a 90 °C water bath and kept reacting for 35 min. To purify the nanoparticles, a 10 kDa Amicon centrifugal filter was first used to concentrate as-synthesized Au-GSH at 6000 rpm (~3700 g) for 8 min, resulting in about 1–2 mL of concentrated Au-GSH. The nanoparticles were then passed through a PD-10 column using PBS as the mobile phase. Fractions 2.5–3.5 mL with a DLS size of 2–3 nm (with Au concentration of ~0.9 mg/mL) was saved for the following studies.

Synthesis of NOTA-Au-GSH

Reduced glutathione is a tripeptide with a gamma peptide linkage between the carboxyl group of the glutamate side-chain and the amine group of cysteine (which is attached by normal peptide linkage to a glycine). The conjugation of NOTA to Au-GSH was achieved by reacting p-SCN-Bn-NOTA with amine groups from the Au-GSH. In a typical synthesis, 6 μL of p-SCN-Bn-NOTA (5 mg/mL in dimethyl sulfoxide) was added into 125 μL of Au-GSH PBS solution. The pH was then adjusted to 8–9 and kept reacting for 1 h at room temperature before purified by using PD-10 column. As-synthesized NOTA-Au-GSH can be stored in 4 °C for more than 2 weeks.

Copper-64 radiolabeling and serum stability studies

To synthesize ^{64}Cu-NOTA-Au-GSH, $^{64}CuCl_2$ (4 mCi, or 148 MBq) was diluted in 300 μL of 0.1 M sodium acetate buffer (pH 6.5) and added to 200 μL NOTA-Au-GSH. The reaction was allowed to proceed at 37 °C for 30 min with constant shaking. Before purification, EDTA (5 μL, 50 mM) was added to chelate all free ^{64}Cu in the mixture. The mixture was shaked at 37 °C for another 5 min. After that, ^{64}Cu-NOTA-Au-GSH was purified using PD-10 columns with PBS as the mobile phase. The radioactivity fractions (typically between 3.0 and 4.0 mL, total of 1 mL) were collected for further *in vivo* PET imaging experiments. The labeling was found to be over 90% (n>5).

For serum stability studies, ^{64}Cu-NOTA-Au-GSH was incubated in whole mouse serum at 37 °C for up to 24 h (the time period investigated for serial PET imaging, which is about two half-lives of ^{64}Cu). Portions of the mixture were sampled at different time points and filtered through 10 kDa cutoff filters. The filtrates were collected, and the radioactivity was measured. The percentages of retained (*i.e.* intact) ^{64}Cu on the ^{64}Cu-NOTA-Au-GSH conjugates were calculated using the equation [(total radioactivity - radioactivity in filtrate)/ total radioactivity] × 100 %.

In vivo static PET/CT, dynamic PET imaging and ex vivo biodistribution studies

PET/CT scans at various time points post-injection using a microPET/microCT Inveon rodent model scanner (Siemens Medical SolutionsUSA, Inc.).

For a normal PET imaging, healthy BALB/c mice were each injected with 5–10 MBq (135–270 μCi) of ^{64}Cu-NOTA-Au-GSH *via* tail vein before serial PET scans. For a PET/CT imaging procedure, a mixture of ^{64}Cu-NOTA-Au-GSH (hot) and concentrated NOTA-Au-GSH (cold) was used for the injection. For dynamic scanning, a group of mice (n=4) were injected with 5–10 MBq (135–270 μCi) of ^{64}Cu-NOTA-Au-GSH. A 60-min dynamic scan was performed and framed into 46 frames: 12×5 s, 6×10 s, 6×30 s, 10×60 s, 6×150 s, 5×300 s. Image reconstruction, and region of interest (ROI) analysis of the PET data were performed similar as described previously.[17–19] Quantitative PET data were presented as percentage of the injected dose per gram (%ID/g). For biodistribution study, major organs were collected and wet-weighted at 24 h post-injection. The radioactivity in the tissue was measured using a gamma-counter (Perkin-Elmer) and presented as %ID/g (mean ± SD).

In vivo clearance study using metabolic cages

To quantitatively study the clearance rate of ^{64}Cu-NOTA-Au-GSH, a group of mice (n=3) mice were injected with ~1.85 MBq (~50 μCi) of ^{64}Cu-NOTA-Au-GSH. Mice were then kept individually in its own metabolic cage. Mouse urine and feces were collected separately at different time points (6 h, 16 h and 24 h) post-injection. The activities in the urine and feces were counted by a gamma-counter and decayed back to the injection time. The radioactivity in organs was measured using a gamma-counter (Perkin-Elmer) and presented as %ID (mean ± SD).

Supplementary Material

Refer to Web version on PubMed Central for supplementary material.

Acknowledgments

This work is supported, in part, by the University of Wisconsin - Madison, the National Institutes of Health (NIBIB/NCI 1R01CA169365, P30CA014520, T32CA009206 and 5T32GM08349), the National Science Foundation (DGE-1256259), and the American Cancer Society (125246-RSG-13-099-01-CCE).

References

1. Song J, Yang X, Jacobson O, Huang P, Sun X, Lin L, Yan X, Niu G, Ma Q, Chen X. Adv Mater. 2015; 27:4910. [PubMed: 26198622]

2. Fan W, Bu W, Shen B, He Q, Cui Z, Liu Y, Zheng X, Zhao K, Shi J. Adv Mater. 2015; 27:4155. [PubMed: 26058562]
3. Chen H, Wang GD, Chuang YJ, Zhen Z, Chen X, Biddinger P, Hao Z, Liu F, Shen B, Pan Z, Xie J. Nano Lett. 2015; 15:2249. [PubMed: 25756781]
4. Chen F, Hong H, Goel S, Graves SA, Orbay H, Ehlerding EB, Shi S, Theuer CP, Nickles RJ, Cai W. ACS Nano. 2015; 9:3926. [PubMed: 25843647]
5. Hong H, Shi J, Yang Y, Zhang Y, Engle JW, Nickles RJ, Wang X, Cai W. Nano Lett. 2011; 11:3744. [PubMed: 21823599]
6. Yang K, Zhang S, Zhang G, Sun X, Lee ST, Liu Z. Nano Lett. 2010; 10:3318. [PubMed: 20684528]
7. Bardhan R, Chen W, Bartels M, Perez-Torres C, Botero MF, McAninch RW, Contreras A, Schiff R, Pautler RG, Halas NJ, Joshi A. Nano Lett. 2010; 10:4920. [PubMed: 21090693]
8. Burns AA, Vider J, Ow H, Herz E, Penate-Medina O, Baumgart M, Larson SM, Wiesner U, Bradbury M. Nano Lett. 2009; 9:442. [PubMed: 19099455]
9. Benezra M, Penate-Medina O, Zanzonico PB, Schaer D, Ow H, Burns A, DeStanchina E, Longo V, Herz E, Iyer S, Wolchok J, Larson SM, Wiesner U, Bradbury MS. J Clin Invest. 2011; 121:2768. [PubMed: 21670497]
10. Phillips E, Penate-Medina O, Zanzonico PB, Carvajal RD, Mohan P, Ye Y, Humm J, Gonen M, Kalaigian H, Schoder H, Strauss HW, Larson SM, Wiesner U, Bradbury MS. Sci Transl Med. 2014; 6:260ra149.
11. Longmire M, Choyke PL, Kobayashi H. Nanomedicine (Lond). 2008; 3:703. [PubMed: 18817471]
12. Liu J, Yu M, Zhou C, Yang S, Ning X, Zheng J. J Am Chem Soc. 2013; 135:4978. [PubMed: 23506476]
13. Liu J, Yu M, Ning X, Zhou C, Yang S, Zheng J. Angew Chem Int Ed Engl. 2013; 52:12572. [PubMed: 24123783]
14. Zhou C, Hao G, Thomas P, Liu J, Yu M, Sun S, Oz OK, Sun X, Zheng J. Angew Chem Int Ed Engl. 2012; 51:10118. [PubMed: 22961978]
15. Zhou C, Long M, Qin Y, Sun X, Zheng J. Angew Chem Int Ed Engl. 2011; 50:3168. [PubMed: 21374769]
16. Soo Choi H, Liu W, Misra P, Tanaka E, Zimmer JP, Itty Ipe B, Bawendi MG, Frangioni JV. Nat Biotech. 2007; 25:1165.
17. Engle JW, Hong H, Zhang Y, Valdovinos HF, Myklejord DV, Barnhart TE, Theuer CP, Nickles RJ, Cai W. Mol Pharm. 2012; 9:1441. [PubMed: 22519890]
18. Zhang Y, Hong H, Engle JW, Yang Y, Barnhart TE, Cai W. Am J Nucl Med Mol Imaging. 2012; 2:1. [PubMed: 22229128]
19. Shi S, Yang K, Hong H, Valdovinos HF, Nayak TR, Zhang Y, Theuer CP, Barnhart TE, Liu Z, Cai W. Biomaterials. 2013; 34:3002. [PubMed: 23374706]

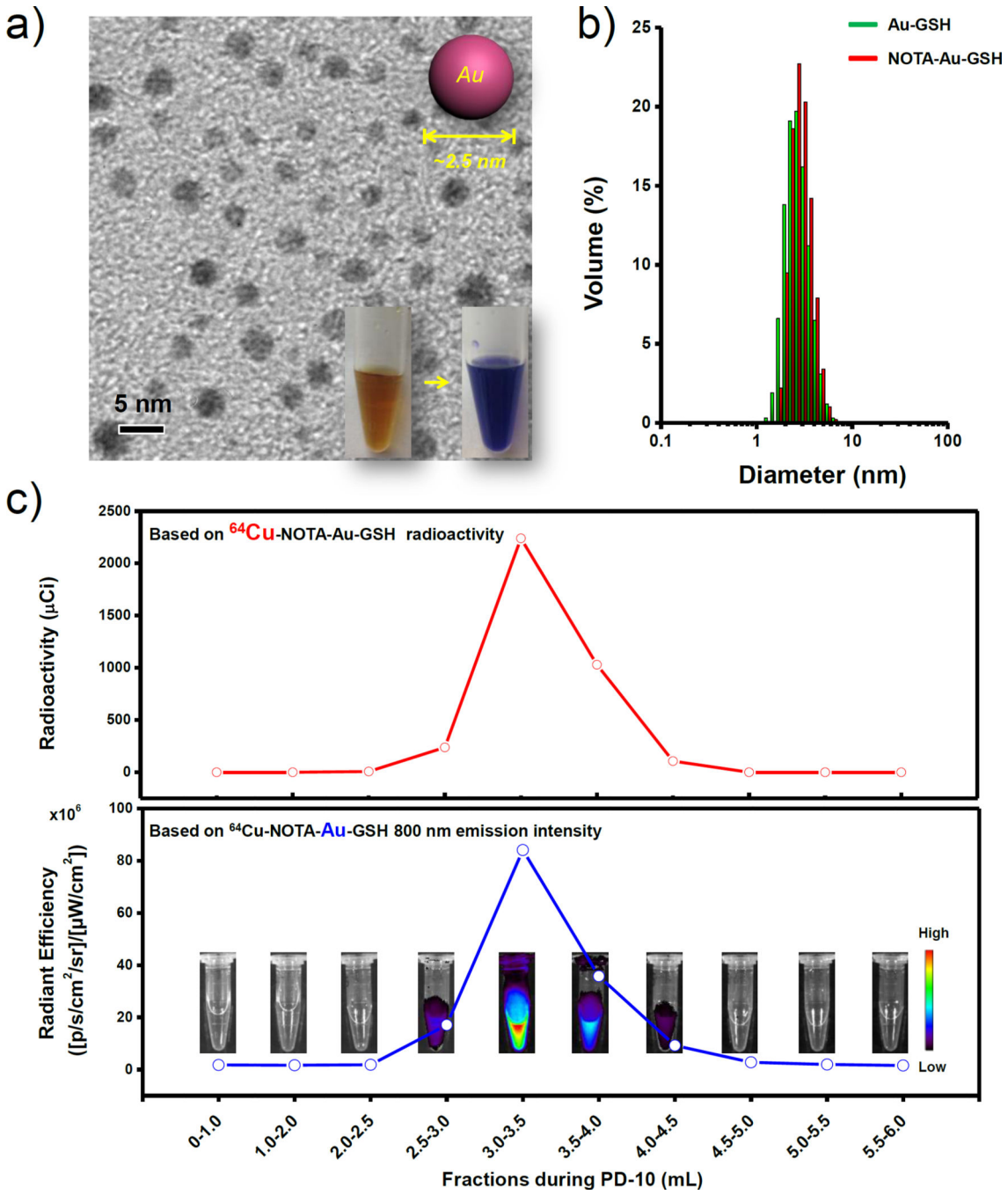

Figure 1. Synthesis and characterization of Au-GSH nanoparticles

(**a**) A representative transmission electron microscopy (TEM) image of 2–3 nm sized Au-GSH. Inset (upper right) is a schematic illustration of Au-GSH. Inset (lower right) is an amine group testing showing the color changing of solution from light yellow to blue after adding ninhydrin. (**b**) DLS size distribution of Au-GSH (HD size: 2.5 ± 0.1 nm) and NOTA-Au-GSH (HD size: 2.6 ± 0.1 nm). (**c**) Elution profiles based on ^{64}Cu radioactivity (up) and Au nanoparticles 800 nm emission intensities of ^{64}Cu-NOTA-Au-GSH (down). The inset

shows the optical images of different fractions after the PD-10 column. Over 90% of ^{64}Cu-NOTA-Au-GSH was eluted between 3.0 and 4.0 mL.

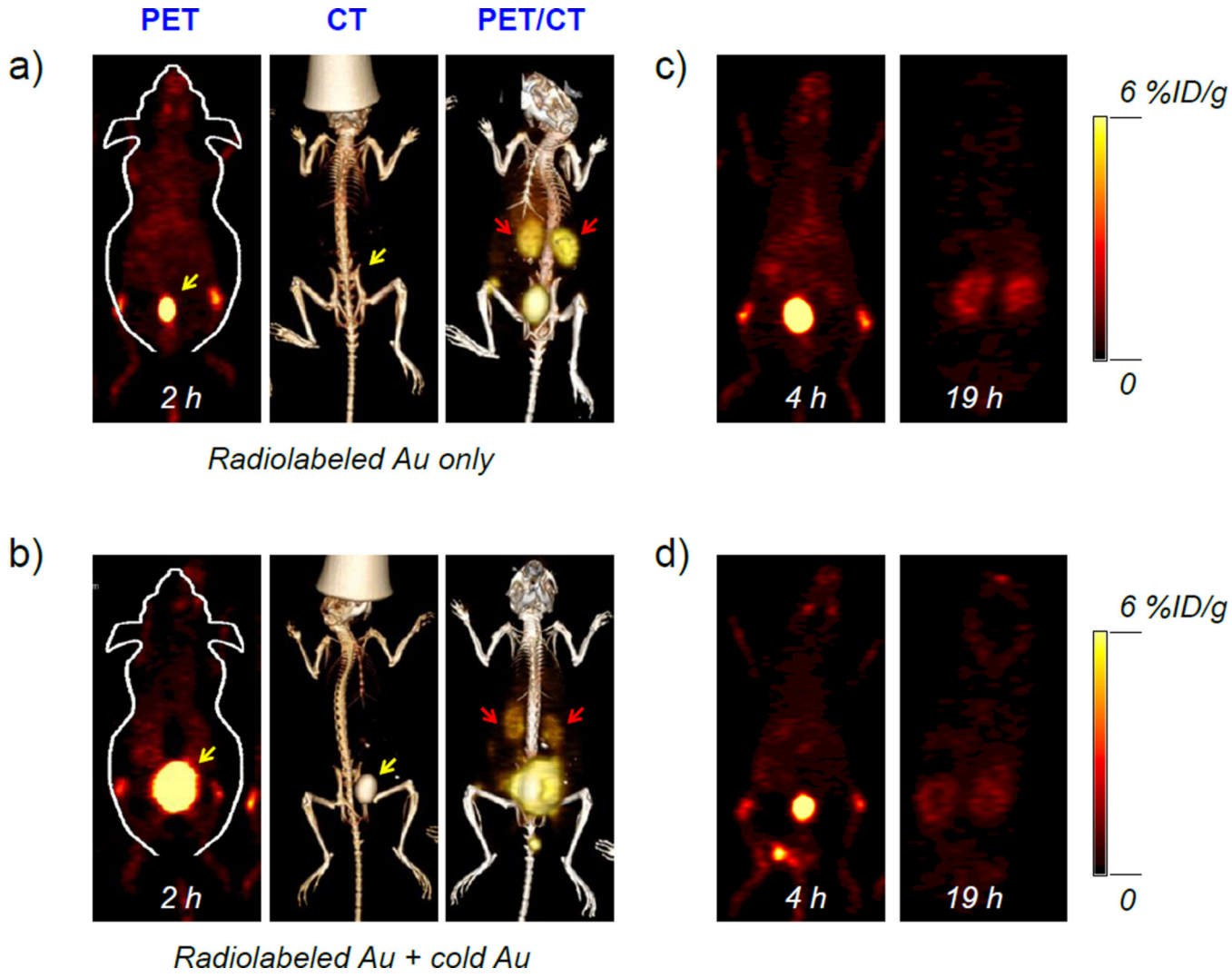

Figure 2. ***In vivo*** **PET/CT imaging of ^{64}Cu-NOTA-Au-GSH**

From left to right: PET, CT and PET/CT imaging of BALB/c mouse injected with (**a**) only radiolabeled Au-GSH (^{64}Cu-NOTA-Au-GSH, ~200 μCi/mouse) at 2 h post-injection, and (**b**) radiolabeled Au-GSH (^{64}Cu-NOTA-Au-GSH, ~200 μCi/mouse) and cold Au (NOTA-Au-GSH, ~0.5 mg/mouse) at 2 h post-injection. PET imaging of BALB/c mouse injected with (**c**) only radiolabeled Au-GSH (^{64}Cu-NOTA-Au-GSH) at 4 h and 19 h post-injection, and (**d**) radiolabeled Au-GSH (^{64}Cu-NOTA-Au-GSH) and cold Au (NOTA-Au-GSH) at 4 h and 19 h post-injection. The bladder was marked with a yellow arrow, while kidneys were marked with red arrows.

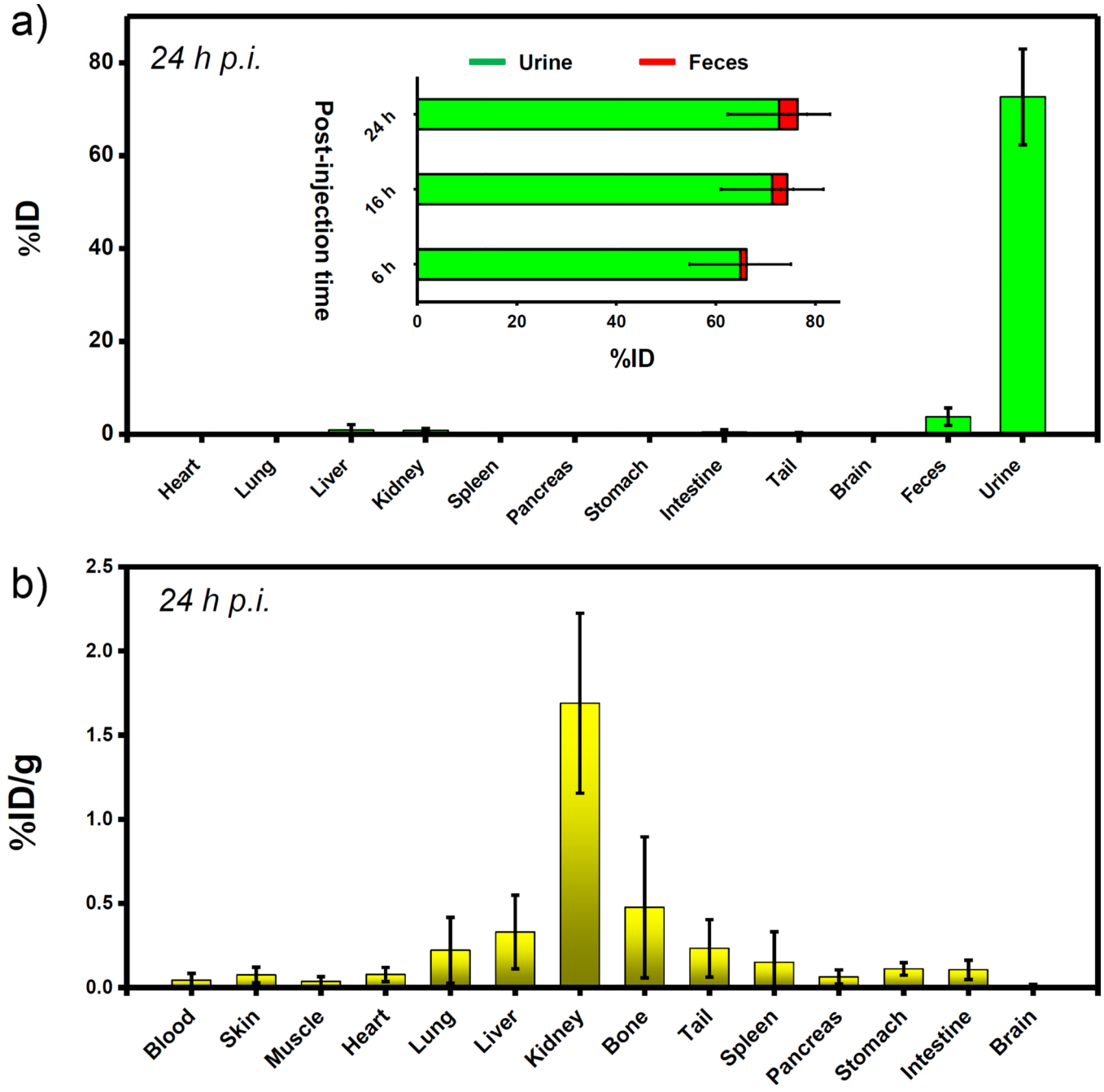

Figure 3. ***In vivo*** **clearance and biodistribution studies**

(**a**) Biodistribution of mice (n=3) from the metabolic cage clearance study (24 h post-injection). Organ uptake was presented as %ID. The inset shows renal (green, urine) and hepatic clearance (red, feces) clearance ^{64}Cu-NOTA-Au-GSH at different post-injection time points. (**b**) Biodistribution of mice (n=4) at 24 h post-injection. Organ uptake was presented as %ID/g.

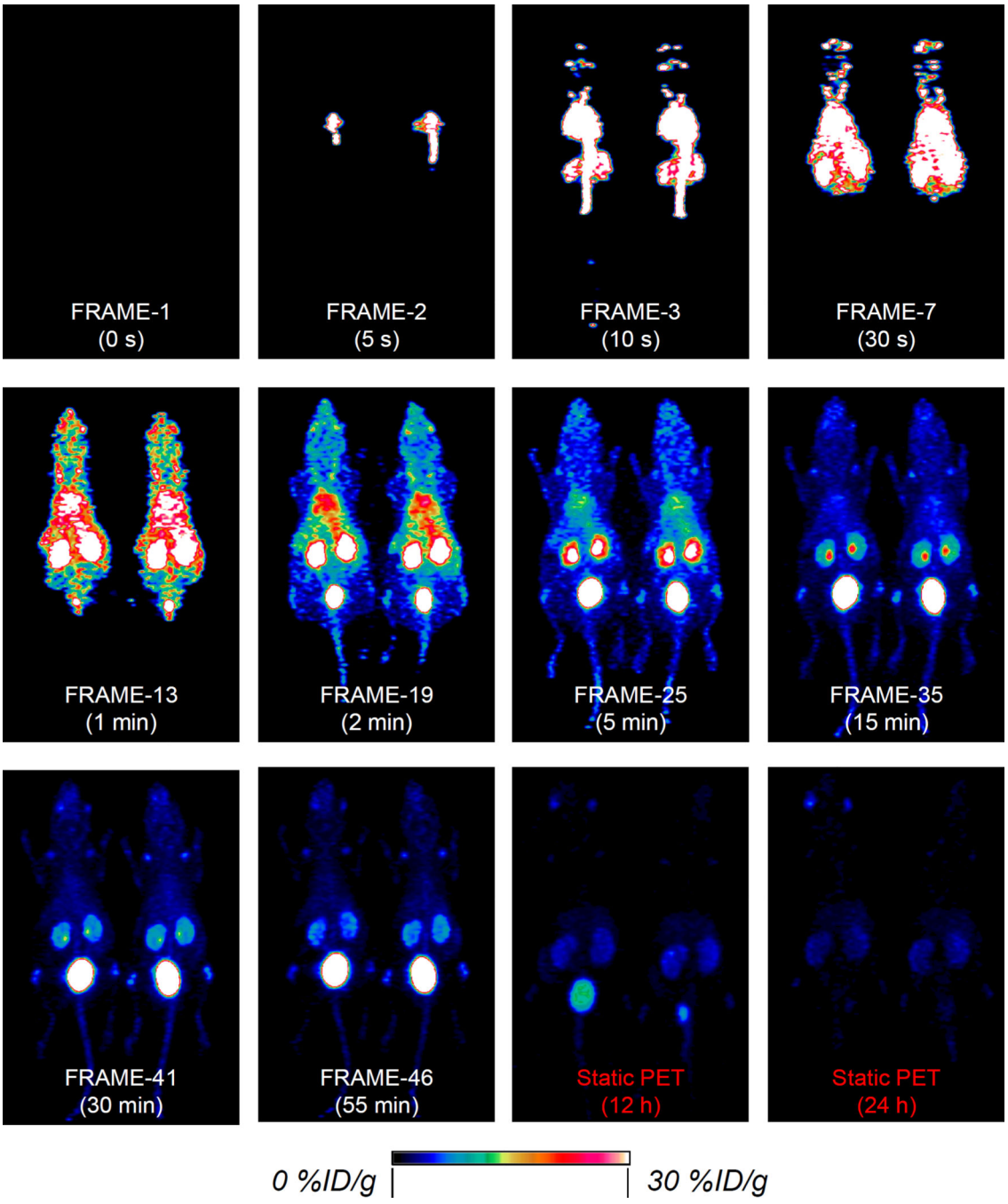

Figure 4. Dynamic PET imaging of ^{64}Cu-NOTA-Au-GSH

Selected frames showing the maximum intensity projection images from dynamic PET imaging of mice injected with ^{64}Cu-NOTA-Au-GSH. The last two images were from static PET imaging of the same mice at 12 h and 24 h post-injection. Only 2 out of 4 mice are shown here.

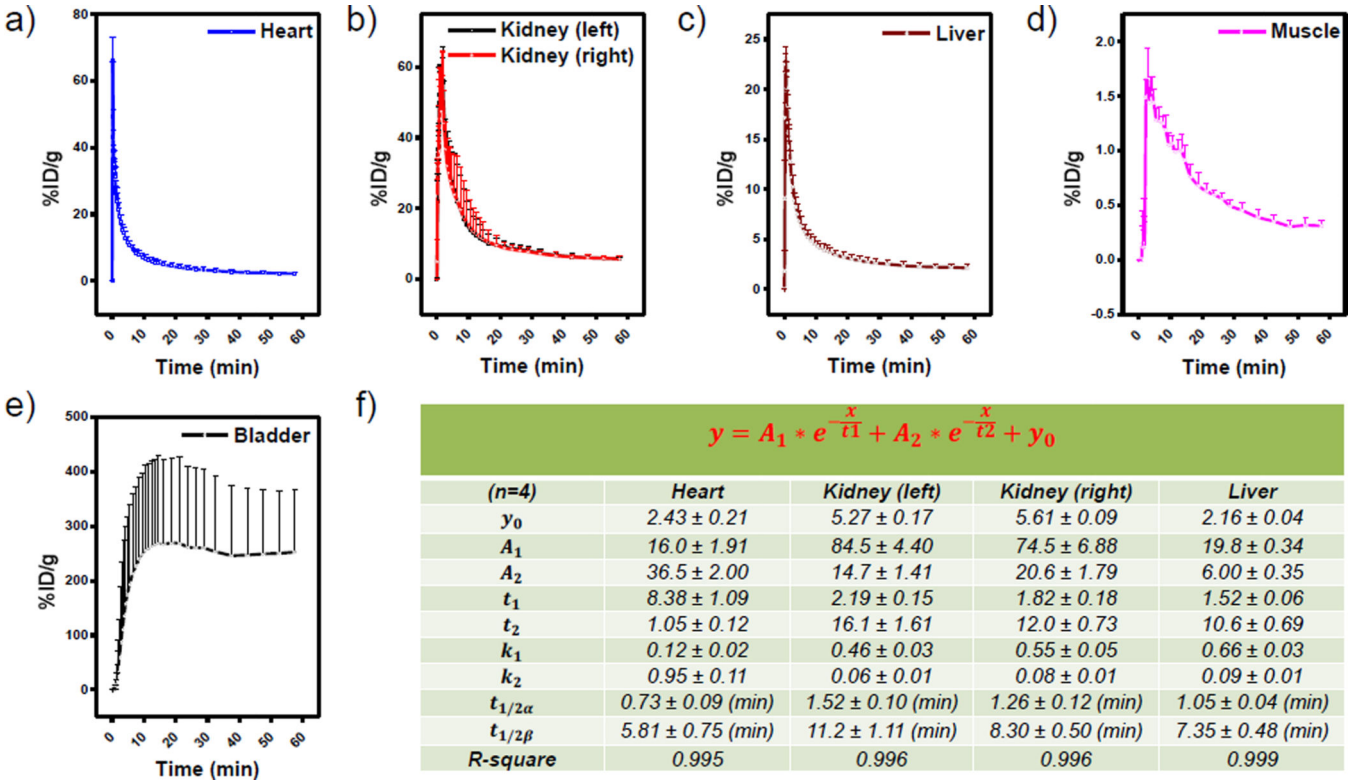

f)

$$y = A_1 * e^{-\frac{x}{t1}} + A_2 * e^{-\frac{x}{t2}} + y_0$$

(n=4)	Heart	Kidney (left)	Kidney (right)	Liver
y_0	2.43 ± 0.21	5.27 ± 0.17	5.61 ± 0.09	2.16 ± 0.04
A_1	16.0 ± 1.91	84.5 ± 4.40	74.5 ± 6.88	19.8 ± 0.34
A_2	36.5 ± 2.00	14.7 ± 1.41	20.6 ± 1.79	6.00 ± 0.35
t_1	8.38 ± 1.09	2.19 ± 0.15	1.82 ± 0.18	1.52 ± 0.06
t_2	1.05 ± 0.12	16.1 ± 1.61	12.0 ± 0.73	10.6 ± 0.69
k_1	0.12 ± 0.02	0.46 ± 0.03	0.55 ± 0.05	0.66 ± 0.03
k_2	0.95 ± 0.11	0.06 ± 0.01	0.08 ± 0.01	0.09 ± 0.01
$t_{1/2\alpha}$	0.73 ± 0.09 (min)	1.52 ± 0.10 (min)	1.26 ± 0.12 (min)	1.05 ± 0.04 (min)
$t_{1/2\beta}$	5.81 ± 0.75 (min)	11.2 ± 1.11 (min)	8.30 ± 0.50 (min)	7.35 ± 0.48 (min)
R-square	0.995	0.996	0.996	0.999

Figure 5.

Time-activity curves of ^{64}Cu-NOTA-Au-GSH in different major organs of (**a**) heart, (**b**) two kidneys, (**c**) liver, (**d**) muscle and (**e**) bladder. (**f**) A table summarizes the two-compartment model fitting results of ^{64}Cu-NOTA-Au-GSH in different organs.